# Bifurcation of potential vorticity gradients across the Southern Hemisphere stratospheric polar vortex.

Jonathan Conway[1], Greg Bodeker[1], and Chris Cameron[1]

[1]Bodeker Scientific, 42 Russell Street, Alexandra, 9320, New Zealand

*Correspondence to:* J.P. Conway (jono@bodekerscientific.com)

**Abstract.** The winter-time stratospheric westerly winds circling the Antarctic continent, also known as the Southern Hemisphere polar vortex, create a barrier to mixing of air between middle and high latitudes. This dynamical isolation has important consequences for export of ozone-depleted air from the Antarctic stratosphere to lower latitudes. The prevailing view of this dynamical barrier has been an annulus compromising steep gradients of potential vorticity (PV) that create a single semi-permeable barrier to mixing. Analyses presented here show that this barrier often displays a bifurcated structure where a doubled-walled barrier exists. The bifurcated structure manifests as enhanced gradients of PV at two distinct latitudes - usually on the inside and outside flanks of the region of highest wind speed. Metrics that quantify the bifurcated nature of the vortex have been developed and their variation in space and time has been analysed. At most isentropic levels between 370K and 850K, bifurcation is strongest in winter and reduces dramatically during spring. From August onwards a distinct structure emerges, where elevated bifurcation remains between 475K and 600K, and a mostly single walled barrier occurs at other levels. While bifurcation at a given level evolves from month to month, and does not always persist through a season, inter-annual variations in the strength of bifurcation display coherence across multiple levels in any given month. Accounting for bifurcation allows the region of reduced mixing to be better characterized. These results suggest that improved understanding of cross-vortex mixing requires consideration of the polar vortex not as a single mixing barrier, but as a barrier with internal structure that is likely to manifest as more complex gradients in trace gas concentrations across the vortex barrier region.

## 1 Introduction

The polar vortex is the defining dynamical feature of the stratosphere during winter and early spring. The steep gradients in trace gas concentrations and in dynamical tracers such as potential vorticity (PV) across the vortex boundary region indicate a dynamical barrier to the mixing of air between the mid-latitude and the high latitude stratosphere (Hoskins et al., 1985, Plumb and Ko, 1992). In the Southern Hemisphere, during winter and spring, the barrier isolates cold stratospheric air formed in the polar night from warmer mid-latitude air. The polar stratospheric clouds that form in this region provide the conditions needed for the heterogenous chemical reactions that create the halogen radicals that go on to deplete ozone (Solomon, 1999). In springtime, the barrier prevents ozone depleted air within the polar vortex from mixing with ozone rich air that accumulates in the downward branch of the Brewer-Dobson circulation equatorward of the vortex. By defining the location of the polar vortex in equivalent latitude (EL) coordinates (Butchart and Remsberg, 1986), the temporal evolution of the size and strength

of this dynamical containment of ozone depletion can be assessed (Bodeker et al., 2002) and periodic mixing of air masses into and out of the vortex can be identified (Manney and Lawrence, 2016). Providing a quantitative description of the vortex barrier also allows the representation of the polar vortex in coupled chemistry-climate models to be evaluated (Struthers et al., 2009).

The centre of the vortex boundary region is most often defined as the location of the maximum gradient of PV with respect to EL (herein referred to as PV gradient), with the caveat that the true peak is also located in the region of the maximum westerly jet (Nash et al., 1996). Bodeker et al. (2002) formalised this method by defining meridional impermeability as the product of the PV gradient and the average wind speed in the same EL coordinates. Because there is a one-to-one correspondence between PV values and EL (see Figure 1a of Nash et al., 1996), identifying the EL of the centre of the vortex boundary region allows the PV value corresponding to the centre of the vortex boundary region to be ascertained. This allows polar vortex tracking algorithms (e.g. Manney and Lawrence, 2016) to map the size and location of the vortex in latitude-longitude coordinates. Because of the temporal variability in the vortex, these methods sometimes rely on climatological PV gradients to define PV values that correspond to the centre of the vortex boundary region (Manney and Lawrence, 2016). The inner and outer edges of the vortex boundary region can be defined using the second derivative of PV with respect to EL. These edges can then be combined with trajectory model calculations to quantify transport into and out of the vortex boundary region (Paparella et al., 1997). The vortex boundary can also be defined by calculating the gradient of trace gas concentrations in the same EL coordinates as PV, through Lagrangian metrics such as the Lyapunov exponents (Garny et al., 2007), or the complexity of tracer gradients through effective diffusivity (Haynes and Shuckburgh, 2000). Because of the minimal computational requirements, the PV gradient is an attractive method to define the vortex boundary region.

The increased resolution of recent reanalyses now allows us to resolve the structure of PV gradients in EL coordinates around the polar vortex in much finer detail than was available when the Nash et al. (1996) definition was proposed. This paper investigates PV gradients during late winter and spring over the altitude range where the highest rates of Southern Hemisphere ozone depletion occur (mid-stratosphere). The aim of this paper is to characterise, in detail, the Southern Hemisphere polar vortex dynamical barrier, including the vertical and latitudinal structure, seasonal evolution and internal structure of the vortex boundary region.

## 2 Methods

### 2.1 Data sets

The primary data set used in this paper is the ERA-Interim reanalysis (Dee et al., 2011) produced by the European Centre for Medium-Range Weather Forecasting (ECMWF). This reanalysis uses a 4D variational assimilation system to combine observed climate variables in a dynamically consistent fashion. Zonal and meridional wind speed, and Ertel potential vorticity (PV) data were downloaded on nine potential temperature ($\Theta$) levels (350K, 370K, 395K, 430K, 475K, 530K, 600K, 700K, 850K) from the ECWMF online archive on a regular latitude-longitude grid with a resolution of 0.75° in both dimensions. To ensure that features observed in ERA-Interim are not unique to a single reanalysis, data from the National Centers for Environmental Prediction (NCEP) Climate Forecast System Reanalysis (CFSR; Saha et al., 2010) and its continuation, the Climate Forecast

System version 2 (CFSv2; Saha et al., 2014), were also analysed. For simplicity, the combination of these two NCEP data sets are referred to here as CFSR, though we note slight changes in model parameterizations between CFSR and CFSv2 (see Saha et al., 2014). Zonal and meridional wind speed, temperature and Ertel PV fields from CFSR were downloaded on six $\Theta$ levels (350K, 400K, 450K, 550K, 650K, 850K) on a 0.5° regular latitude-longitude grid. To facilitate comparison of PV gradients

5 on different $\Theta$ levels, PV was scaled to have a similar range of values throughout the stratosphere using the scaling factor $\Theta/\Theta_0^{-9/2}$ (Lait, 1994), with a reference level ($\Theta_0$) of 350K. For ease, PV is also presented here in PVU ($10^6 Km^2 kg^{-1} s^{-1}$), referred to as sPVU when PV has been scaled according to Lait (1994).

## 2.2 Detection of bifurcated PV gradient

PV gradients across the polar vortex were calculated by first determining the one-to-one relationship between PV and EL for

10 each time step in the reanalyses (6 hourly). EL is the true latitude that would enclose the same area as that enclosed by a given PV contour (Butchart and Remsberg, 1986). Here, EL was determined for 181 PV steps between the maximum and minimum PV at each time step, using percentile steps to avoid spurious zero values of PV gradient that occur when no PV data falls between two successive PV steps.

To characterise the bifurcation of the vortex barrier, an algorithm was developed to detect secondary peaks in PV gradient

15 as follows (see also Figure 1a):

- The primary peak is identified by the largest value of PV gradient between -40° and -80° equivalent latitude.

- A secondary peak is identified as a local maximum in PV gradient that exceeds a fraction (peak ratio) of the primary peak, that is located a sufficient distance (separation) from the primary peak. In addition, the PV gradient between the two peaks must decrease by a fraction (dip fraction) of the secondary peak in PV gradient.

20 A bifurcation index (BI) is derived using combinations of peak ratio and dip fraction that are increasingly restrictive as shown in Table 1. Single peaks are denoted as BI = 0 when the peak ratio is less than 0.5 or the dip fraction is less than 0.05. Two choices of separation (2° and 5°) were analysed for all results. Apart from the expected increase in the fraction of bifurcated profiles detected and smaller average BI for 2° separation, the results do not change substantially. The more restrictive 5° separation is used hereafter to highlight the structure of moderate to strong bifurcation. The dip fraction was found to have

25 more influence in determining BI than peak ratio. Large peak ratios occur in profiles assessed with small to moderate BI, whereas the dip fraction closely follows the threshold values used to define BI (not shown). Thus, profiles assessed with small to moderate BI can range from two closely matched peaks with only a small interstitial dip, to a much smaller secondary peak on the shoulder of the primary peak.

The inner and outer edges of the vortex boundary region were calculated following Nash (1996); the inner and outer edges

30 are evaluated as the local maximum and minimum in the second derivative of PV with respect to EL around the location of the peak in PV gradient, respectively (Figure 1b). Note that the sign of the second derivative is opposite to the description in Nash et al. (1996) because of the negative sign convention for EL in the Southern Hemisphere. For bifurcated profiles, we nuance
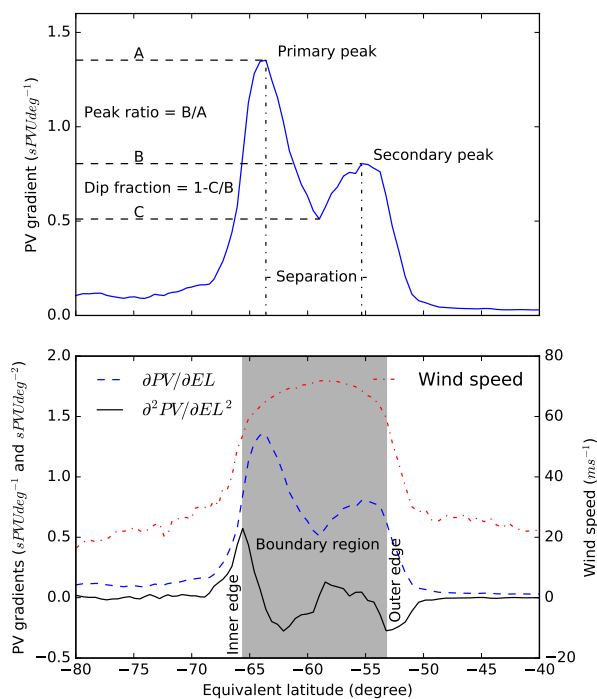
**Figure 1.** Example of (a) the calculation of the peak ratio, dip fraction and separation from a meridional profile of PV gradient ($\partial PV/\partial EL$) and (b) the calculation of inner and outer edges of the vortex boundary region from $\partial^2 PV/\partial EL^2$ ($sPVU deg^{-2}$), with wind speed ($ms^{-1}$) and $\partial PV/\partial EL$ ($sPVU deg^{-1}$) also shown for reference. This example is a profile at 530K on 1 September 2007 from ERA-Interim.

**Table 1.** Threshold values of peak ratio and dip fraction used to define the bifurcation index (BI).

| Bifurcation Index | Peak Ratio | | Dip Fraction |
|:---:|:---:|:---:|:---:|
| 0 | $< 0.5$ | or | $< 0.05$ |
| 1 | $>= 0.5$ | and | $>= 0.05$ |
| 2 | $>= 0.55$ | and | $>= 0.1$ |
| 3 | $>= 0.6$ | and | $>= 0.15$ |
| 4 | $>= 0.65$ | and | $>= 0.2$ |
| 5 | $>= 0.7$ | and | $>= 0.25$ |
| 6 | $>= 0.75$ | and | $>= 0.3$ |
| 7 | $>= 0.8$ | and | $>= 0.35$ |
| 8 | $>= 0.85$ | and | $>= 0.4$ |
| 9 | $>= 0.9$ | and | $>= 0.45$ |
| 10 | $>= 0.95$ | and | $>= 0.5$ |

the Nash et al. (1996) definition by evaluating the inner edge around the poleward peak and outer edge around the equatorward peak.

## 3   Results

### 3.1   Structure of meridional PV gradients in ERA-Interim

5  Figure 2 shows the climatological mean (1979-2016) structure of PV gradients across the polar vortex during the winter and spring. Large PV gradients generally align with the region of enhanced wind speed, which is largest at high levels during mid-winter. In August and September, PV gradients intensify in concert with the region of strong wind speed becoming predominately confined to latitudes poleward of -50°. At mid-levels, between 475K and 600K, two regions of enhanced PV gradient are visible, aligned with the inside and outside edges of the region of maximum wind speed (Figure 2c, d). As spring

10  progresses, the vortex barrier region narrows and the end of October only a single region of elevated PV gradients remains.
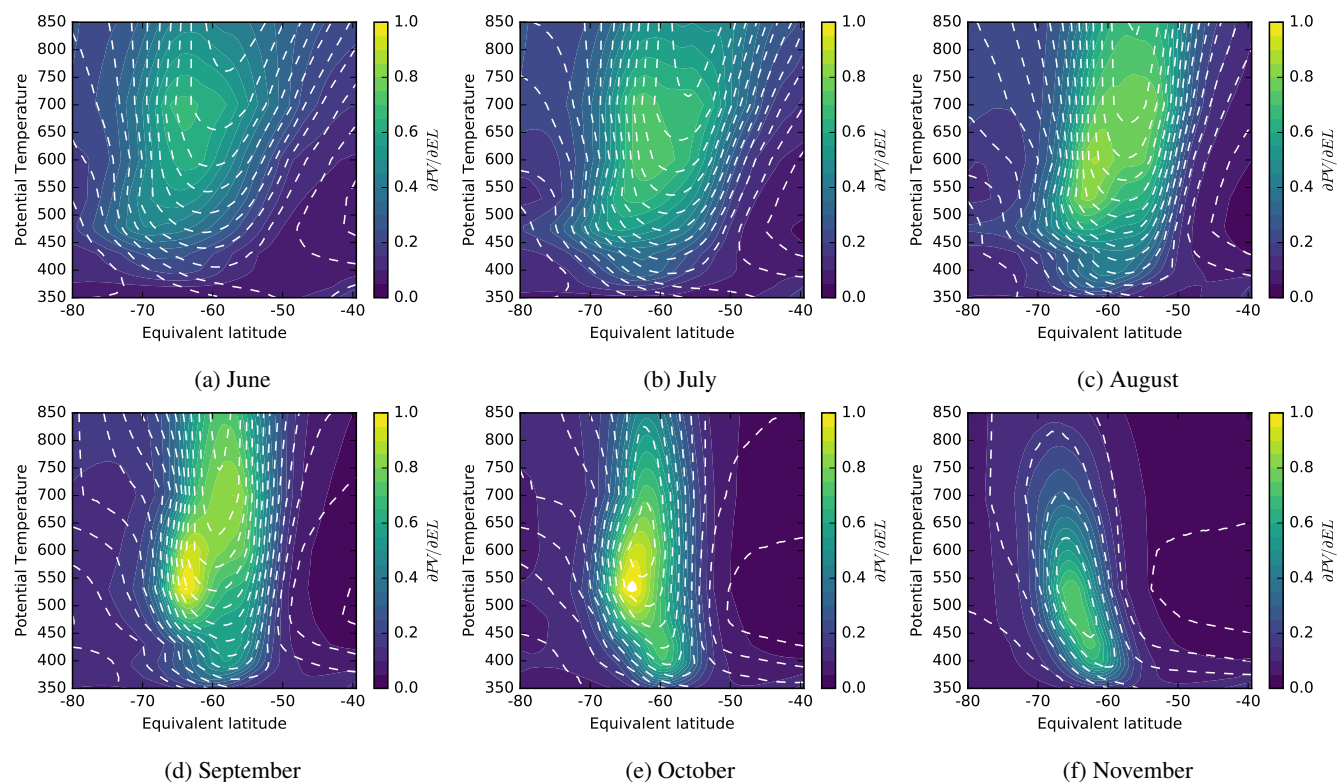
**Figure 2.** Average PV gradient (colours; $sPVUdeg^{-1}$) and wind speed (dashed lines; in 10 ms$^{-1}$ steps) at ERA-Interim levels between 350K and 850K, for selected months, 1979-2016.

Considering individual years, the bifurcation of PV gradients with respect to EL becomes more apparent. The characteristic evolution of the bifurcated structure is clearly illustrated during the year 2007 (Figure 3). The PV gradient displays two distinct peaks aligned with the inside and outside flanks of the region of maximum wind speed, while the region at the wind speed maximum has notably reduced PV gradients. The bifurcation of PV gradients is not mirrored in the wind speed, which display

5    only a single broad region of maximum wind speed. Moderate to high BI is established at most levels during winter, but moderate BI remains only at mid-levels as PV gradients intensify during spring (Figure 3c).

|  (a) August PV gradients  |  (b) September PV gradients  |  (c) Bifurcation Index  |
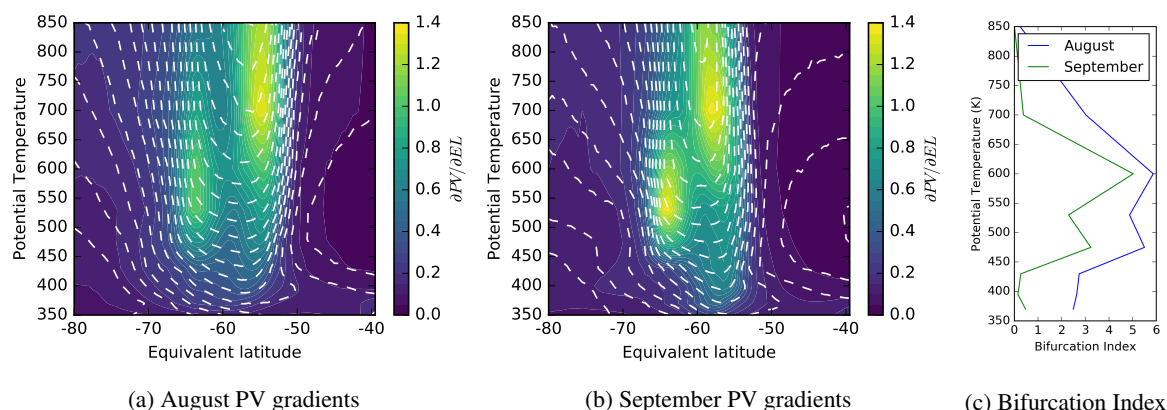
**Figure 3.** Average PV gradient (colours; $sPVU deg^{-1}$) and wind speed (dashed lines; in 10 ms$^{-1}$ steps) during (a) August and (b) September 2007 at ERA-Interim levels between 350K and 850K. Also shown is (c) mean BI at each level for each month.

## 3.2    Bifurcation metrics

Generally, early and mid-winter show high average BI, with BI weakening from August onwards (Figure 4a). Low BI during October and November indicates that the vortex barrier has only a single peak, or is weakly bifurcated. The exception is mid-

10    levels (475K to 600K), where elevated BI remains through September, and, to a lesser extent, October. During September, the barrier is more often than not bifurcated at these levels (Figure 4b). At all levels, the average separation between primary and secondary peaks reduces through the season from around 10° in June to around 5° in October (Figure 4c). During the winter, there is only a slight tendency for secondary peaks to occur equatorward of primary peaks (Figure 4d). As spring progresses a more defined spatial structure develops; at mid-levels the secondary peak is most often equatorward of the primary peak, while

15    at other levels the secondary peak is more often poleward of the primary peak. The small BI at low and high levels (Figure 4a) indicate that secondary peaks at these levels are either weaker and not as common as those at mid-levels. Maximum values of peak ratio occur during September at 475K and 600K, indicating that two peaks with similar magnitude occur frequently at these levels (Figure 4e). The general decline in dip fraction over the season mirrors the decline in BI, showing its strong influence on BI (Figure 4f).
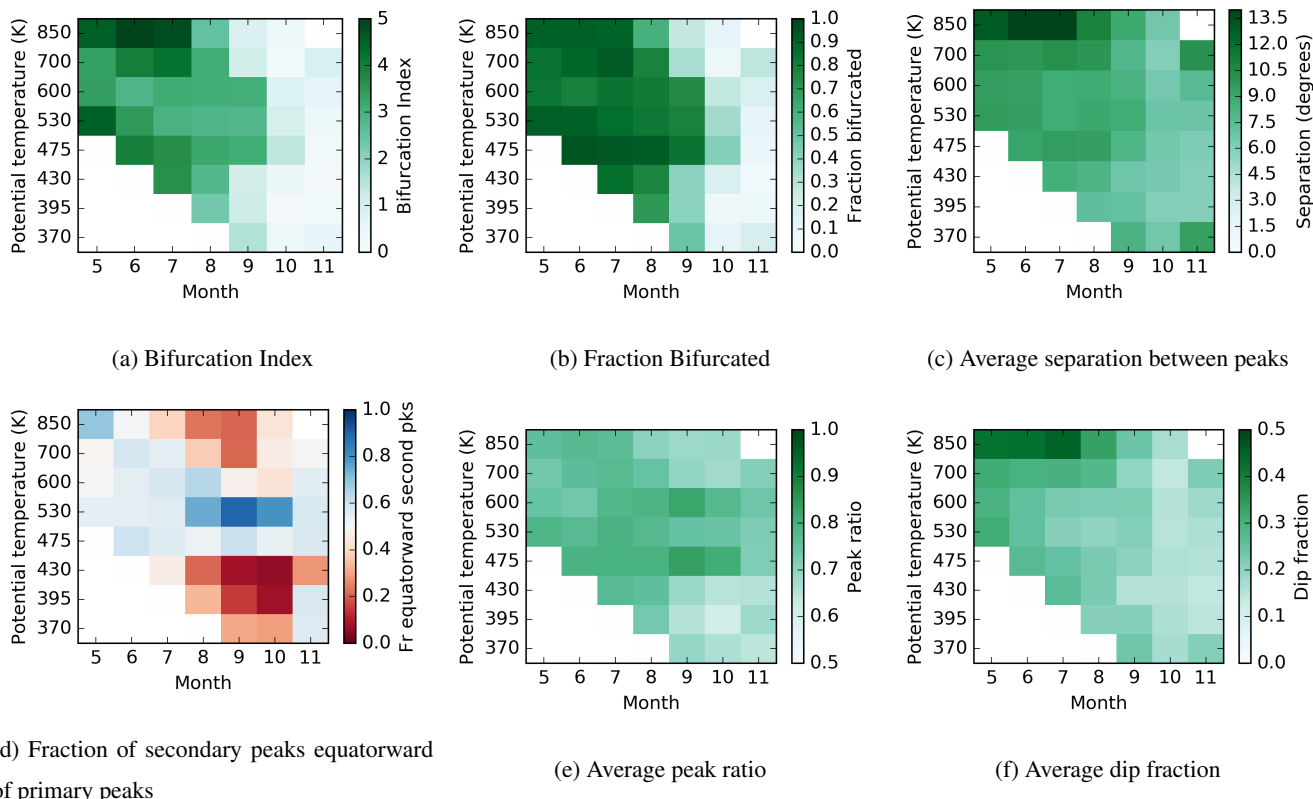
**Figure 4.** Climatological structure and seasonal evolution of bifurcation metrics derived at ERA-Interim levels between 370K and 850K, 1979-2016. Data is only shown for months in which the climatological vortex is well developed at a given level, identified by an average maximum PV gradient > 0.45 sPVU deg$^{-1}$.

## 3.3 Location of primary and secondary peaks

The locations of primary and secondary peaks in PV gradient have a well-defined structure during spring. At mid-levels (475K to 600K), peaks in PV gradient occur in two preferred locations centred around -63° and -55° (Figure 5), with primary peaks being most often in the poleward location, and secondary peaks in the equatorward location. Earlier in the season, the locations

5   of primary peaks are more dispersed, especially at higher levels (700K and 850K). At lower levels (370K to 430K), primary peaks are more tightly clustered around -60° and secondary peaks tend to be to poleward of primary peaks.

## 3.4 Inter-annual variability in bifurcation

Large inter-annual variations in BI display some coherence across multiple levels (Figure 6). For example, during July, when bifurcation is common, anomalously low BI occurs simultaneously over multiple levels in a given year (e.g. 1992, 2008).

10  During September, vertically coherent inter-annual variations in BI occur at mid-levels, with anomalies in BI that extend
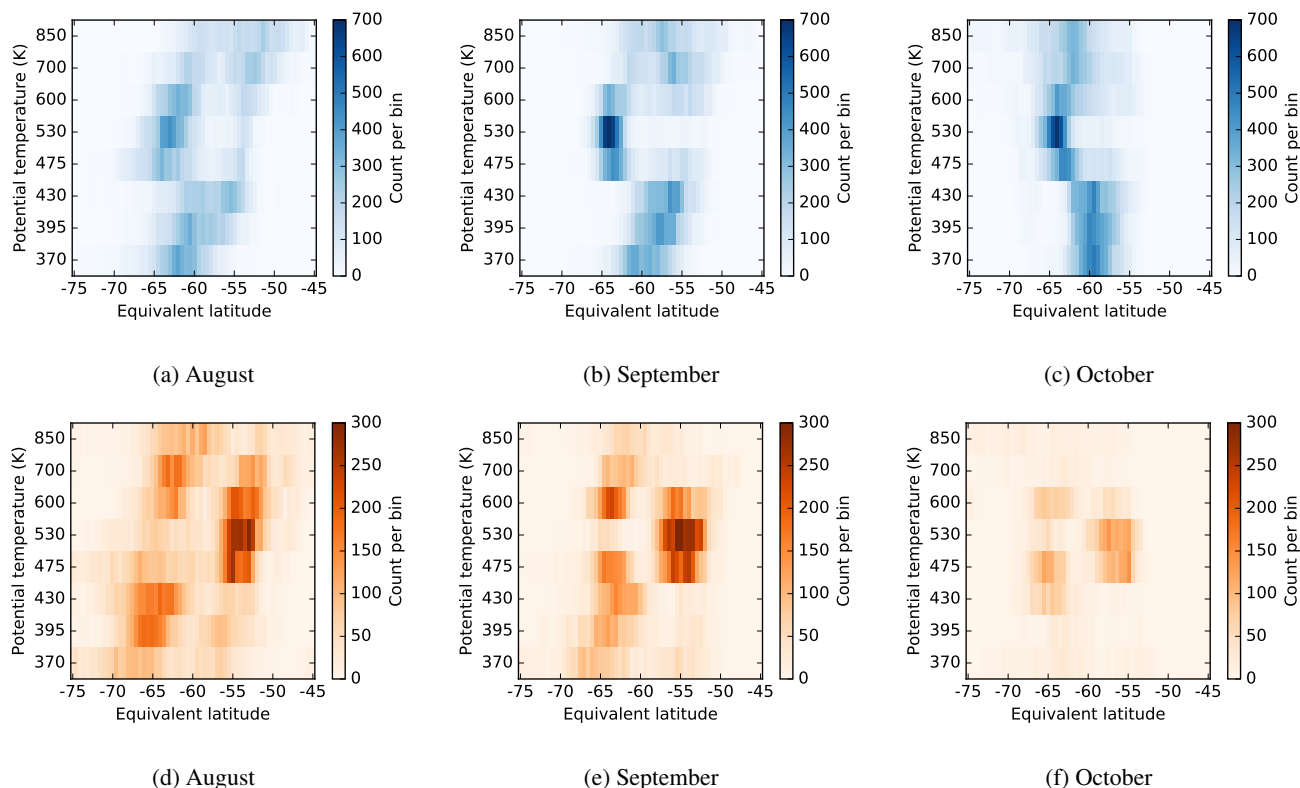
**Figure 5.** Locations of (a-c) primary and (d-f) secondary peaks in PV gradient at ERA-Interim levels between 370K and 850K, 1979-2016. Peaks are selected using a minimum separation of 5° and the colour scale shows the number of time steps that peaks occurred in each 0.5° bin.

through multiple levels and weak BI above and below. In November, the single-wall barrier predominates and bifurcation is only seen in some years.

## 4   Discussion

### 4.1   Comparison with CFSR

5   Average BI calculated from CFSR shows a similar structure to that observed in ERA-Interim (Figure 7). Bifurcation generally decreases during the spring, but remains strong at 550K and 650K. The tendency for secondary peaks to occur equatorward of primary peaks is restricted to the 550K layer, with 650K and 450K layers displaying similar structure to those at 700K and 430K in ERA-Interim, respectively. The average locations of primary and secondary peaks are similar, with the primary peaks at 550K being most often in the poleward position (-63°) during September (Figure 8). At 650K and 450K, primary peaks

10   are most often situated at an equatorward location (around -55° to -58°). The occurrence of bifurcation in a second reanalyses
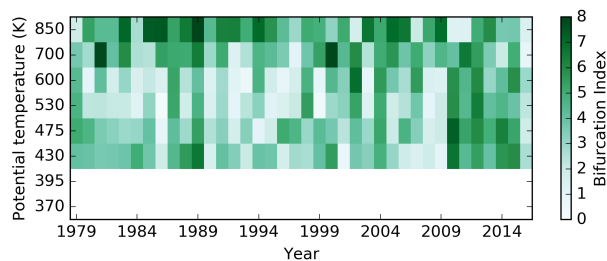
(a) July
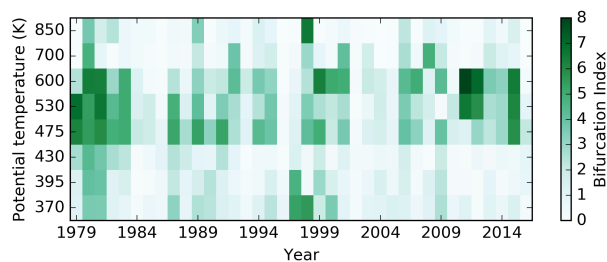
(b) September
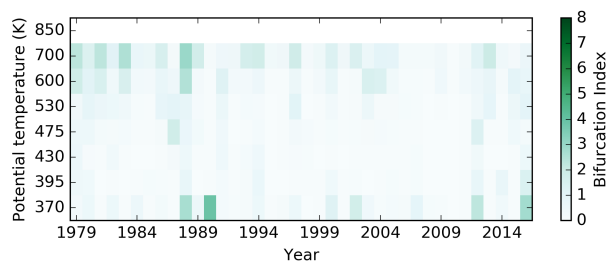
(c) November

**Figure 6.** Time series of monthly average BI at ERA-Interim levels between 370K and 850K, 1979-2016. Data is only shown at levels in which the climatological vortex is well developed in a given month - see Figure 4 caption.

gives us confidence that the patterns observed are real phenomena and not artefacts of the production of a particular reanalysis data set.

## 4.2 Impacts of bifurcated PV gradients

The bifurcation of PV gradients across the Southern Hemisphere polar vortex represents a pause in the rapid meridional increase
5    in PV that occurs across the vortex barrier. Even though PV gradients weaken between the poleward and equatorward peaks, they are still substantially larger than those in the mid-latitudes or the vortex interior. The most rapid decreases in PV occur at the points where relative vorticity also displays the most rapid decrease - in the transition from the positive vorticity associated

(a) Bifurcation Index

(b) Fraction of secondary peaks equatorward of primary peaks
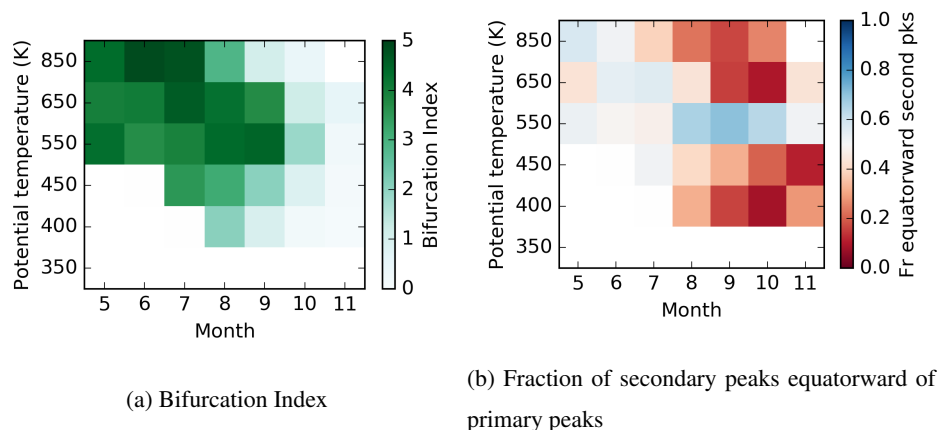
**Figure 7.** Climatological structure and seasonal evolution of bifurcation metrics at CFSR levels between 350K and 850K, 1979-2016. Data are only shown for months in which the climatological vortex is well developed at a given level - see Figure 4 caption.

(a) September

(b) September
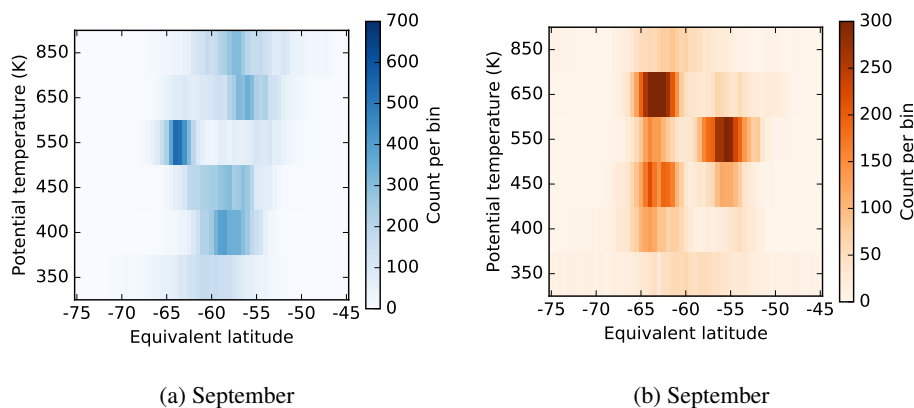
**Figure 8.** Location of (a) primary and (b) secondary peaks in PV gradient at CFSR levels between 350K and 850K, 1979-2016. Peaks are selected using a minimum separation of 5° and the colour scale shows the number of time steps that peaks occurred in each 0.5° bin.

with increasing wind speed on the outer flank of the vortex, and to the large negative vorticity associated with decreasing wind speed on the inner flank of the vortex (see example Figure 9). Thus, bifurcation of PV gradients appears to be caused by the separation of two distinct zones of rapidly decreasing relative vorticity. Gradients of absolute vorticity follow closely those in relative vorticity, while the vertical gradient of Θ does not display any obvious bifurcation. During periods where the barrier is
5 narrow, the two zones of enhanced vorticity gradient coalesce and only a single peak in PV gradient remains.

The weakening of PV gradients within the vortex barrier during periods of bifurcation may increase mixing within the vortex boundary region, while still reducing the transport of material through the barrier as a whole. This could lead to more complex variations of trace gas concentrations across the barrier. With a single (narrower) barrier, there is less efficient mixing of air and steeper gradients in trace gas concentrations within the vortex barrier region would be expected.
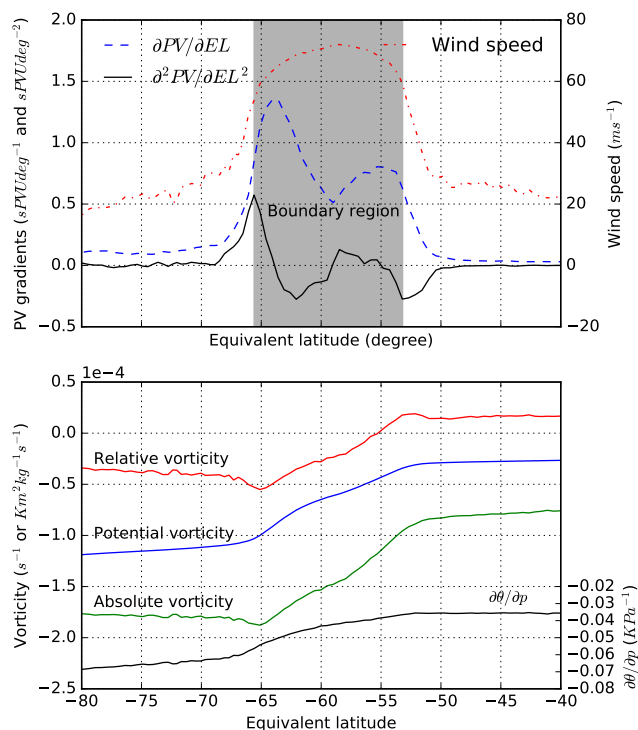
**Figure 9.** Example meridional profiles of (a) (LH axis) gradients of PV with respect to EL ($\partial PV/\partial EL$ ($sPVUdeg^{-1}$) and $\partial^2 PV/\partial EL^2$ ($sPVUdeg^{-2}$)) and (RH axis) wind speed ($ms^{-1}$), and (b) (LH axis) absolute and relative vorticity ($s^{-1}$), PV ($Km^2kg^{-1}s^{-1}$), and (RH axis) vertical gradient of potential temperature ($KPa^{-1}$). All lines are averages at EL calculated from PV. This example is a profile at 530K on 1 September 2007 from ERA-Interim.

Increased PV gradients observed at mid-levels during spring, on the inner flank of the vortex barrier (Figure 5b), align with the outer limits of regions of enhanced ozone loss (Lee et al., 2001, Bodeker et al., 2002). This provides motivation for updated analyses of trends in vortex attributes, such as BI, to provide context for recent trends in ozone concentrations observed during September (e.g. Solomon et al., 2016).

5    ## 4.3    Redefining a vortex barrier region

If a single vortex 'edge' is defined according to Nash et al. (1996), bifurcation can lead to spurious changes in the location of the vortex boundary region over time. In cases where the PV gradient has two peaks of similar magnitude, the location of the 'edge' will flip-flop from one location to the other over the course of a few days, while clearly the vortex has not rapidly changed in size. This challenges interpretations of the vortex 'edge' that define a single location at the maximum PV gradient.

10    By using the bifurcation algorithm described above to detect secondary peaks in the PV gradient, a more realistic and robust analysis of the location of vortex barrier is made possible.

The Nash et al. (1996) definition of the vortex boundary region is also challenged by the bifurcated structure. The vortex boundary cannot be simply thought of as the region between the local maximum and local minimum in the second derivative of PV with respect to EL around the location of the primary peak in PV gradient. The presence of secondary peaks in PV gradient inside or outside the primary peak highlights that region of limited mixing is, in fact, much wider than that analysed around only the primary peak.

(a) August        (b) September        (c) October
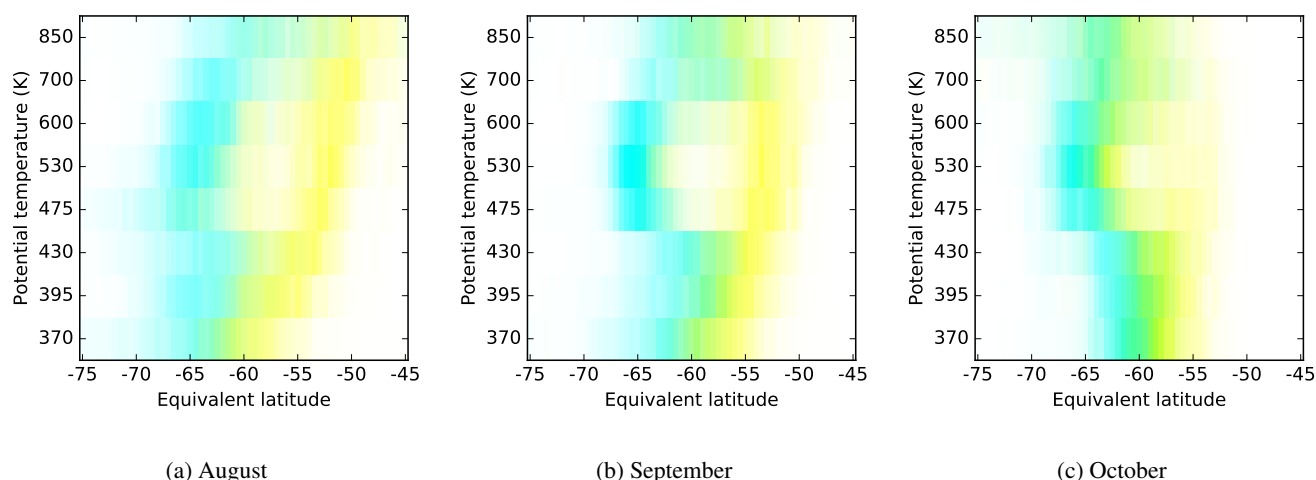
**Figure 10.** Location of inner (cyan) and outer (yellow) edges of the vortex boundary region at ERA-Interim levels between 370K and 850K, 1979-2016. The vortex boundary region is defined using the criteria of Nash et al. (1996) but also accounts for secondary peaks in PV gradient. The intensity of cyan and yellow represents the frequency of inner and outer boundaries in each 0.5° bin, respectively, with green colours indicating a mix of both inner and outer boundaries at different times. The frequency per bin is scaled with respect to a maximum count of 600 per bin.

When the bifurcation is taken into account, the width of the vortex boundary region becomes much larger than that analysed with the Nash et al. (1996) definition (Figure 10). During August and September, a clear separation between inner and outer edges becomes apparent at mid-levels. The inner edge is predominately around -65°, with the outer edge at around -52° to -54°. At times, the outer edge is poleward of -60°, but the inner edge is rarely equatorward of -60°. At lower levels the boundary region is usually confined to a small area around the primary peak at -60°, while at higher levels, the location and width of the boundary region are much more variable. As spring progresses the boundary region coalesces at all levels.

This study suggests there is a need to redefine the location of the vortex barrier as a boundary region in which mixing is reduced below some critical threshold, rather than as a single 'edge'. This definition would demarcate only the inner and outer edges of the vortex boundary region, and would not be dependent on defining a single vortex 'edge'. If a single EL or PV value is needed to demarcate the vortex, then the average EL of the boundary region could still be calculated, but this value would be more robust against bifurcation than a single 'edge'. The extension of the Nash et al. (1996) methodology shown here shows promise. Defining threshold values of PV gradient may also be a useful way to define the barrier region, though a

formal comparison with other metrics of isentropic mixing (e.g. effective diffusivity, Lyapunov exponents) is warranted. This comparison would allow complementary values of each metric to demarcate the inner and outer edges to be inferred.

## 5 Conclusions

The strength of the dynamical isolation of high-latitude air caused by the Southern Hemisphere polar vortex has been analysed
5 using gradients of potential vorticity along equivalent latitude coordinates for nine isentropic levels between 350K and 850K in the ERA-Interim reanalysis. Analyses presented here show that this barrier often displays a bifurcated structure where, rather than a single barrier to meridional mixing, a doubled-walled barrier exists. The bifurcated structure manifests as enhanced gradients of potential vorticity at two distinct equivalent latitudes - usually the inside and outside flanks of the region of highest wind speed.

10  Metrics quantifying the bifurcated nature of the vortex barrier have been developed and their variation in space and time has been analysed. While the height-latitude structure differs from year to year, bifurcation appears to be a persistent feature of the vortex barrier region. It was found that at most isentropic levels between 370K and 850K, bifurcation is strongest in winter and reduces dramatically during spring. From August onwards, a distinct structure emerges, with stronger bifurcation at mid-levels (475K to 600K) and a mostly single-walled barrier at other levels. While the strength of the bifurcation at a given level evolves
15 from month to month and does not always persist through a season, inter-annual variations display coherence across multiple levels in any given month. The detection of secondary peaks in PV gradient permits a more realistic view of the true region of weak mixing associated with the polar vortex.

The results presented above suggest that improved understanding of cross-vortex mixing requires consideration of the polar vortex not as a single mixing barrier, but as a barrier with internal structure that is likely to manifest as more complex gradients
20 in trace gas concentrations across the vortex boundary region. More work is needed to quantify relationships between PV gradients and other metrics of mixing (effective diffusivity, Lyapunov exponents) as well as identify the interactions between the structure of PV gradients, ozone and temperature. Analyses of trends in bifurcation should also be pursued to provide context to observed trends in ozone concentrations during springtime.

*Data availability.* The ERA-Interim data set used in this paper is available from the ECMWF online archives: http://apps.ecmwf.int/datasets.
25 The CFSR and CFSv2 data sets are available from https://rda.ucar.edu/datasets/ds093.0/ and https://rda.ucar.edu/datasets/ds094.0/, respectively.

*Author contributions.* JC developed and performed the analyses, and prepared the manuscript with contributions from all co-authors.

*Competing interests.* The authors declare that they have no conflict of interest.

*Acknowledgements.* This research was funded by a Royal Society of New Zealand Marsden Fund research grant titled "The permeability of the Antarctic vortex", contract number BDS1401.

# References

Bodeker, G. E., Struthers, H., and Connor, B. J.: Dynamical containment of Antarctic ozone depletion, Geophysical Research Letters, 29, 1098, https://doi.org/10.1029/2001gl014206, 2002.

Butchart, N. and Remsberg, E. E.: The area of the stratospheric polar vortex as a diagnostic for tracer transport on an isentropic surface, Journal of Atmospheric Sciences, 43, 1319–1339, https://doi.org/10.1175/1520-0469(1986)043<1319:TAOTSP>2.0.CO;2, 1986.

Dee, D. P., Uppala, S. M., Simmons, A. J., Berrisford, P., Poli, P., Kobayashi, S., Andrae, U., Balmaseda, M. A., Balsamo, G., Bauer, P., Bechtold, P., Beljaars, A. C. M., van de Berg, L., Bidlot, J., Bormann, N., Delsol, C., Dragani, R., Fuentes, M., Geer, A. J., Haimberger, L., Healy, S. B., Hersbach, H., Hólm, E. V., Isaksen, L., Kållberg, P., Köhler, M., Matricardi, M., McNally, A. P., Monge-Sanz, B. M., Morcrette, J. J., Park, B. K., Peubey, C., de Rosnay, P., Tavolato, C., Thépaut, J. N., and Vitart, F.: The ERA-Interim reanalysis: configuration and performance of the data assimilation system, Quarterly Journal of the Royal Meteorological Society, 137, 553–597, https://doi.org/10.1002/qj.828, 2011.

Garny, H., Bodeker, G. E., and Dameris, M.: Trends and variability in stratospheric mixing: 1979–2005, Atmospheric Chemistry and Physics, 7, 5611–5624, https://doi.org/10.5194/acp-7-5611-2007, 2007.

Haynes, P. and Shuckburgh, E.: Effective diffusivity as a diagnostic of atmospheric transport: 1. Stratosphere, Journal of Geophysical Research: Atmospheres, 105, 22 777–22 794, https://doi.org/10.1029/2000jd900093, 2000.

Hoskins, B., McIntyre, M., and Robertson, A.: On the use and significance of isentropic potential vorticity maps, Quarterly Journal of the Royal Meteorological Society, 111, 877–946, https://doi.org/10.1002/qj.49711147002, 1985.

Lait, L.: An alternative form of Potential Vorticity, Journal of the Atmospheric Sciences, 51, 1754–1759, https://doi.org/10.1175/1520-0469(1994)051<1754:AAFFPV>2.0.CO;2, 1994.

Lee, A., Roscoe, H., Jones, A., Haynes, P., Shuckburgh, E., Morrey, M., and Pumphrey, H.: The impact of the mixing properties within the Antarctic stratospheric vortex on ozone loss in spring, Journal of Geophysical Research, 106, 3203–3211, https://doi.org/10.1029/2000JD900398, 2001.

Manney, G. L. and Lawrence, Z. D.: The major stratospheric final warming in 2016: dispersal of vortex air and termination of Arctic chemical ozone loss, Atmospheric Chemistry and Physics, 16, 15 371–15 396, https://doi.org/10.5194/acp-16-15371-2016, 2016.

Nash, E. R., Newman, P. A., Rosenfield, J. E., and Schoeberl, M. R.: An objective determination of the polar vortex using Ertel's potential vorticity, Journal of Geophysical Research: Atmospheres, 101, 9471–9478, https://doi.org/10.1029/96jd00066, 1996.

Paparella, F., Babiano, A., Basdevant, C., Provenzale, A., and Tanga, P.: A Lagrangian study of the Antarctic polar vortex, Journal of Geophysical Research: Atmospheres, 102, 6765–6773, https://doi.org/10.1029/96jd03377, 1997.

Plumb, R. and Ko, M.: Interrelationships between mixing ratios of long-lived stratospheric constituents, Journal of Geophysical Research, 97, 10 145–10 156, https://doi.org/10.1029/92JD00450, 1992.

Saha, S., Moorthi, S., Pan, H.-L., Wu, X., Wang, J., Nadiga, S., Tripp, P., Kistler, R., Woollen, J., Behringer, D., Liu, H., Stokes, D., Grumbine, R., Gayno, G., Wang, J., Hou, Y.-T., Chuang, H.-Y., Juang, H.-M. H., Sela, J., Iredell, M., Treadon, R., Kleist, D., Van Delst, P., Keyser, D., Derber, J., Ek, M., Meng, J., Wei, H., Yang, R., Lord, S., Van Den Dool, H., Kumar, A., Wang, W., Long, C., Chelliah, M., Xue, Y., Huang, B., Schemm, J.-K., Ebisuzaki, W., Lin, R., Xie, P., Chen, M., Zhou, S., Higgins, W., Zou, C.-Z., Liu, Q., Chen, Y., Han, Y., Cucurull, L., Reynolds, R. W., Rutledge, G., and Goldberg, M.: The NCEP Climate Forecast System Reanalysis, Bulletin of the American Meteorological Society, 91, 1015–1057, https://doi.org/10.1175/2010bams3001.1, 2010.

Saha, S., Moorthi, S., Wu, X., Wang, J., Nadiga, S., Tripp, P., Behringer, D., Hou, Y.-T., Chuang, H.-y., Iredell, M., Ek, M., Meng, J., Yang, R., Mendez, M. P., van den Dool, H., Zhang, Q., Wang, W., Chen, M., and Becker, E.: The NCEP Climate Forecast System Version 2, Journal of Climate, 27, 2185–2208, https://doi.org/10.1175/jcli-d-12-00823.1, 2014.

Solomon, S.: Stratospheric ozone depletion: a review of concepts and history, Reviews of Geophysics, 37, 275–316, https://doi.org/10.1029/1999RG900008, 1999.

Solomon, S., Ivy, D. J., Kinnison, D., Mills, M. J., Neely, R. R., and Schmidt, A.: Emergence of healing in the Antarctic ozone layer, Science, https://doi.org/10.1126/science.aae0061, 2016.

Struthers, H., Bodeker, G. E., Austin, J., Bekki, S., Cionni, I., Dameris, M., Giorgetta, M. A., Grewe, V., Lefèvre, F., Lott, F., Manzini, E., Peter, T., Rozanov, E., and Schraner, M.: The simulation of the Antarctic ozone hole by chemistry-climate models, Atmospheric Chemistry and Physics, 9, 6363–6376, https://doi.org/10.5194/acp-9-6363-2009, 2009.